D. GIULIETTI, S. BASTIANI, T. CECCOTTI, A. GIULIETTI, L.A. GIZZI
and A. MACCHI

Front- and Rear-Face X-Ray Emission from Laser-Irradiated Al Foils.

Estratto da
Il Nuovo Cimento - Vol. 17 D, N. 4 - Aprile 1995 - pp. 401-410

EDITRICE
COMPOSITORI
BOLOGNA
1995

IL NUOVO CIMENTO VOL. 17 D, N. 4 Aprile 1995

Front- and Rear-Face X-Ray Emission from Laser-Irradiated Al Foils.

D. GIULIETTI (1), S. BASTIANI (2), T. CECCOTTI (2), A. GIULIETTI (2)
L. A. GIZZI (2) and A. MACCHI (2)

(1) *Dipartimento di Fisica dell'Università - Piazza Torricelli 2, Pisa, Italy*
(2) *Istituto di Fisica Atomica e Molecolare del CNR - Via del Giardino 7, 56127 Pisa, Italy*

(ricevuto il 20 Dicembre 1994; approvato il 31 Gennaio 1995)

Summary. — We studied the *K*-shell X-ray emission from plasmas produced by laser irradiation of Al foils. Electron temperature and density of the emitting region were estimated from line ratio measurements. Spectra obtained from the rear face of the foils showed that X-ray transmission is influenced by energy transport in the foil.

PACS 52.25 – Plasma properties.
PACS 52.50 – Plasma production and heating.

1. – Introduction.

High-temperature plasmas can be produced by focusing a high-power laser beam on the surface of a solid target. The spectrum of electromagnetic radiation emitted by a hot laser-produced plasma (LPP) includes an X-ray component. At a temperature of hundreds of eV, this component can involve a considerable fraction of the input laser energy.

The basic aspects of X-ray emission from LPPs have been extensively studied both theoretically and experimentally [1]. LPPs have also been studied as bright X-ray sources for application purposes including, for example, lithography, radiography, and shadowgraphy [2] as well as a gain medium for X-ray lasers [3]. The influence of X-ray production on the process of capsule ablation and fuel compression is relevant for Inertial Confinement Fusion (ICF). In addition, X-ray spectroscopy has been a powerful diagnostic tool for LPPs of interest for ICF. Both continuum emission (bremsstrahlung and recombination) and line emission spectra can give information on plasma temperature and density. For this purpose, *K*-shell spectroscopy has been extensively used because spectra are relatively easy to model and analyse.

A satisfactory characterisation of a LPP during its temporal evolution can be obtained using time-resolved X-ray spectroscopy coupled with other diagnostic tools, such as interferometry. This has been recently done to characterise plasmas of

interest for laser-plasma interaction studies [4]. Also a complete theoretical modelling of LPPs requires highly advanced computer simulations [5]. However, time-integrated spectra are very ready to obtain using simple crystal spectrometers and X-ray sensitive films. Comparison of experimental time-integrated spectra with an atomic-physics model can give preliminary information about plasma conditions.

A particular class of measurements has been devoted to X-ray emission from laser-irradiated thin foils. Very thin foils can be used in order to generate plasmas that become underdense during the irradiation with nanosecond laser pulses. In this case X-ray emission can give useful information on the physics of laser interaction with underdense plasmas including, for example, the excitation of electron plasma waves [6].

Thicker foils, for which laser burn-through does not occur, are also interesting targets for different studies. In fact, the emission coming from the rear surface of the foil can be used as an X-ray source to irradiate samples or specimens under conditions virtually free from both laser light and debris. Moreover, the comparison between front and rear X-ray emission can also give important information on transport of radiation energy through the foil.

In this paper we present front- and rear-side X-ray spectra of K-shell emission from laser irradiation of Al foils that were not burnt through during the laser pulse. The investigated spectral region lies between 6 Å and 8 Å wavelength. Plasma density and temperature were estimated by comparison of spectroscopic line ratios with atomic physics simulations. Comparison with hydrodynamic simulations is also discussed. Spectral features of rear-face emission suggest that energy transport through the foil affects the X-ray transmittivity by shifting the photoabsorption edge towards higher energies.

2. – Experimental set-up.

The geometry of the experimental set-up is shown in fig. 1. The plasma was produced in a vacuum chamber by focusing ($f/8$) the beam of a Nd laser ($\lambda = 1.064$ μm) onto several microns thick Al foils. For foil thicknesses of more than 1 μm laser burn-through was not expected to occur.

The Nd laser was transversal monomode and longitudinal multimode. The laser pulse duration was 3 ns (FWHM) and energies up to 2J were delivered on target. The pulse energy was measured shot by shot using a calorimeter which collected a known amount of the beam intensity, coming from the reflection at the interaction chamber window. The size of the laser spot was approximately 60 μm, thus the nominal laser intensity on target was up to $2 \cdot 10^{13}$ W cm^{-2}.

The target was placed along the beam axis close to the beam waist in a position determined by maximizing the signal of an X-ray PIN diode set to detect front emission in the 1–2 keV range. Maximum X-ray intensity was detected with the target placed 1 mm ahead of the beam waist, toward the focusing lens.

X-ray images of the plasma were obtained on film using a pin-hole camera placed in the vertical plane containing the laser beam and looking at the target with an angle of 45 degrees with respect to the beam axis. The spatial resolution of the images was determined by the size of the pin-hole and was about 10 μm.

Spectra were obtained on X-ray sensitive film, employing Bragg diffraction from a PET crystal ($2d = 8.742$ Å). The X-ray conversion efficiency was high enough that

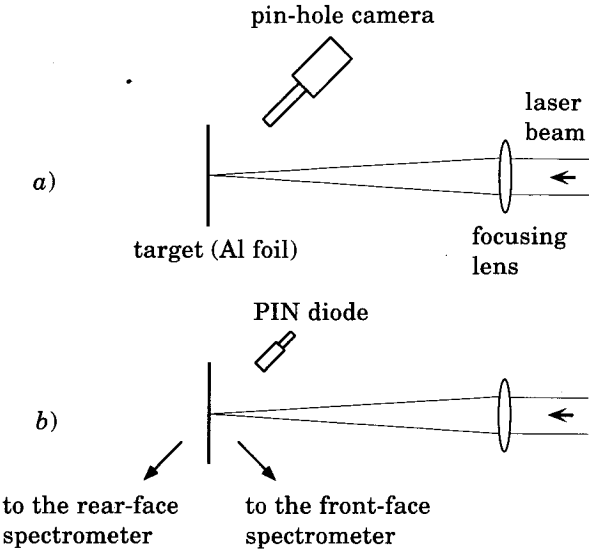

Fig. 1. – Sketch of set-up geometry in the vacuum chamber. The vertical (*a*)) and horizontal (*b*)) planes containing the laser beam axis are shown.

X-ray spectra could be obtained on a single laser shot. All images and spectra were recorded using Kodak DEF [7] film and were analysed using a high-resolution microdensitometer. Be foils were placed in front of the pin-hole and the spectrometer slit to shield the film from visible light. The transmittivity of the Be foils was evaluated using a simple analytic expression, obtained by fitting known values of the X-ray transmittivity for different photon energies [8] with a 3rd-order polynomial.

3. – Results and discussion.

3·1. *Pin-hole images of the source.* – Figure 2 shows a pin-hole camera image of the X-ray emitting plasma. The size of the source was deduced by the FWHM of the lineouts and was found to be about 130 μm in both transverse and longitudinal directions to the laser axis. Since the sensitivity of Kodak DEF film drops dramatically for $\lambda > 13.3$ Å, the spectral components that contribute to the image are those with a wavelength below this value, *i.e.* *K*-shell line and recombination emission and *L*-shell recombination emission.

In the following we will focus the attention on *K*-shell line emission from Al XII and Al XIII ions. The size of the X-ray emitting source is therefore important to estimate opacity effects on X-ray line intensity. Since recombination takes place in the expanding plasma blow-off, the size of the pin-hole image can be considered as an upper limit to the size of the region of emission of *K*-shell line radiation, while a lower limit is given by the size of the laser spot.

3·2. *Analysis of front-face spectra.* – A front-face X-ray spectrum from a 6 μm Al foil in the $6\,\text{Å} < \lambda < 8\,\text{Å}$ wavelength range is shown in fig. 3. This spectrum shows resonance lines from He-α to He-ε and the intercombination line (IC) from Al XII (helium-like) ions and the H-α and H-β from Al XIII (hydrogen-like) ions. We also

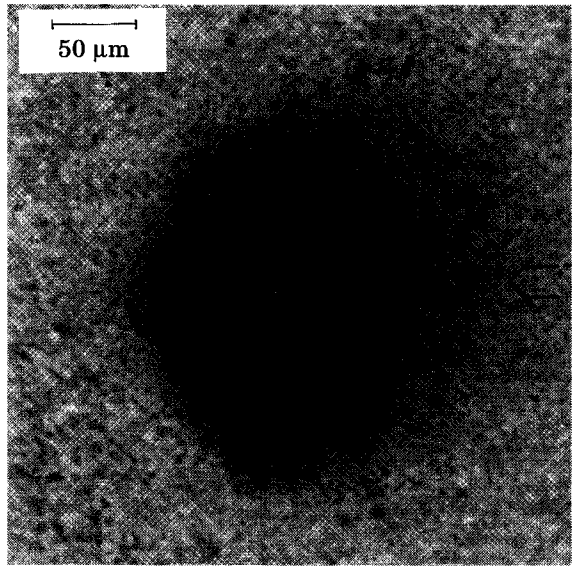

Fig. 2. – Pin-hole camera image of the X-ray source. The horizontal arrow shows the projection of the laser beam axis on the plane of the image. The line of sight of the pin-hole camera is at 45° with respect to the beam axis, as shown in fig. 1.

notice satellite lines on the long wavelength side of He-β and H-α resonance lines due to radiative decay of doubly excited states of Li-like and He-like ions, respectively. The shoulder of the He-α line is due to the lithium-like satellite line arising from the $(1s2p^2)\ ^2S \rightarrow (1s^2 2p)\ ^2P$ transition.

Wavelength calibration was carried out using known values of resonance lines and fitting the dispersion curve (wavelength *vs.* position on the film) with a 3rd-order

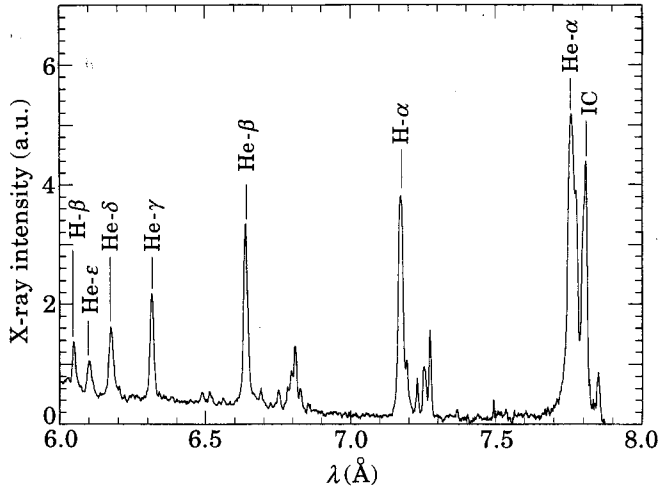

Fig. 3. – Front-face X-ray spectrum from a 6 μm Al foil. The main emission lines are identified.

polynomial; the wavelength values obtained for the satellite lines with this calibration well agree with those given in the literature [9].

The spectral linewidth was due to the finite source size. In fact the spectral resolving power can be approximately given by [10]

$$\lambda/\Delta\lambda = \sqrt{\mathrm{tg}^2\theta_B/(\Delta\theta_c^2 + \Delta y^2/L^2)},$$

where θ_B is the Bragg angle, $\Delta\theta_c \approx 10^{-4}$ is the rocking angle of the PET crystal, $L = 5$ cm is the distance between the source and the crystal plane and $\Delta y \approx 100$ μm is the spatial extent of the source. In our case $\Delta\theta_c^2 \ll \Delta y^2/L^2$, making the source size the leading parameter for $\Delta\lambda/\lambda$. Thus at the centre of the spectrum we find $\Delta\lambda/\lambda \approx$ $\approx 1.5 \cdot 10^{-3}$. Due to this high spectral resolution, eleven different satellite features, corresponding to resolved and unresolved lines, were identified.

3·3. *Temperature and density measurements.* – We used line intensity ratios to determine average values of electron temperature, T_e, and electron density, n_e, of the plasma X-ray emitting region. Experimental line intensities were compared with the predictions of the atomic physics code RATION[11]. This code calculates atomic populations and line intensities assuming collisional-radiative equilibrium (CRE) for a steady-state, homogeneous plasma of given size, temperature and density, including opacity effects. We used the He-δ/H-β ratio $I((1s5p)\,{}^1P \rightarrow$ $\rightarrow (1s^2)\,{}^1S)/I(3p \rightarrow 1s)$ to determine T_e and the He-α/IC ratio $I((1s2p)\,{}^1P \rightarrow$ $\rightarrow (1s^2)\,{}^1S)/I((1s2p)^3P \rightarrow (1s^2)\,{}^1S)$ to determine n_e. This density-sensitive ratio is strongly influenced by opacity effects which make it a double-valued function of n_e [12]. The two values corresponding to our experimental ratio are approximately $10^{21}\,\mathrm{cm}^{-3}$ and $10^{19}\,\mathrm{cm}^{-3}$, respectively. The last value seems unrealistic since it is reasonable that most of the X-ray radiation comes from the plasma region where most of the laser energy is absorbed, *i.e.* close to the critical density for the Nd laser wavelength ($10^{21}\,\mathrm{cm}^{-3}$). To illustrate the influence of opacity effects we give values of T_e and n_e for two different levels of opacity, corresponding to two different choices of the source size. With a plasma size of 50 μm, our experimental line ratios are consistent with $T_e \approx 250$ eV and $n_e \approx 1 \cdot 10^{21}\,\mathrm{cm}^{-3}$, while with a size of 130 μm we obtain $T_e \approx 300$ eV and $n_e \approx 5 \cdot 10^{20}\,\mathrm{cm}^{-3}$.

The model of a homogeneous, stationary plasma is an approximation of the actual laser-produced plasma which is characterised by gradients of T_e and n_e both changing in time.

It has been noted [5] that line spectra spatially averaged along the plasma extent give average values of T_e that are considerably smaller than its maximum value. Also time integration contributes in the same sense, so that the maximum value of T_e in the emission zone could be significantly higher than the average value predicted by our spectra. Also the assumption of steady state requires some discussion. This assumption holds if the atomic processes occur on a time scale faster than that of the hydrodynamics of the plasma. Between all atomic processes, quantitative analysis of the rates shows that ionization and recombination have the longest relaxation time. This time was estimated by calculating the relaxation time of a system with only two levels coupled by ionization and recombination rates. This relaxation time decreases with density and increases with ionization stage. For densities quite close to the critical density and in the temperature range of interest it is less than 1ns, thus justifing the assumption of steady-state plasma. Nevertheless, preliminary

experimental results [13] indicate that the temporal evolution of X-ray emission is modulated by the spikes of the longitudinal multimode laser on a shorter time scale, so that steady-state assumption would require further discussion.

3·4. *Comparison with hydrodynamic simulations.* – We performed hydrodynamic simulations using the 1D code MEDUSA [14]. This code calculates the temporal evolution of plasma hydrodynamic variables for given target and laser pulse. In the simulation a uniform irradiation and a Gaussian pulse are assumed. This does not correspond to our experimental conditions because of intensity dishomogeneities in the laser spot and of the spiky structure of the pulse.

In the hydrodynamic simulations performed at a nominal intensity of $2 \cdot 10^{13}$ W cm^{-2}, the value of T_e at the critical surface is more than 1 keV and the plasma is nearly completely ionized. These values seem to be unrealistic when compared to the experimental results discussed above and suggest that the laser energy converted into internal energy of the plasma could be overestimated. In fact this could be due to the target displacement from the beam waist position as well as to the fact that the code does not account for the amount of energy reflected at the critical surface or scattered by parametric instabilities. Thus it may be more realistic to make a comparison with a simulation at a lower laser intensity. We think that a 50% reduction in laser intensity could give an indication.

In fig. 4 we report the calculated profiles of n_e and T_e at the time of laser pulse peak, for an intensity of $1 \cdot 10^{13}$ W cm^{-2}. The value of T_e at the critical surface is about 550 eV: the plasma still seems to be hotter than predicted by line intensity ratios.

This is not surprising because the 1D hydrodynamic code tends to overestimate both density and temperature, since it cannot account for the actual 3D spread of energy and matter that is evident from X-ray images. The 1D approximation is expected to hold until plasma longitudinal size is less than the size of the laser spot. This is true at times less than R/c_s, where R is the size of the spot and c_s is the speed

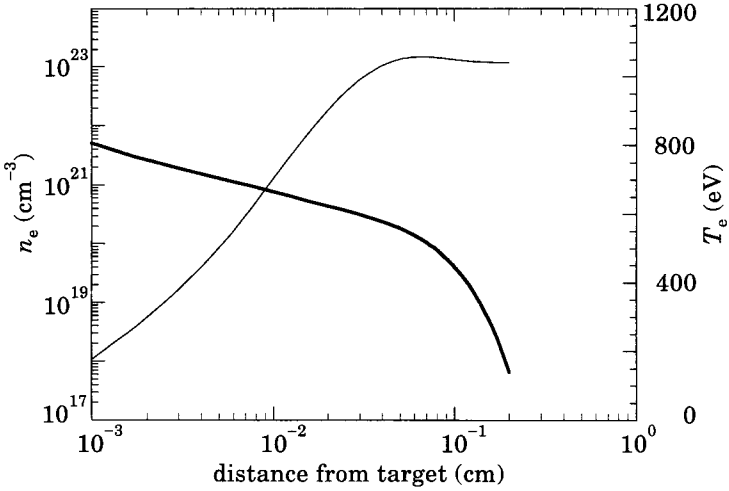

Fig. 4. – Calculated profiles of electron temperature (thin line) and density (thick line) at the peak of the laser power, for an intensity of $1 \cdot 10^{13}$ W cm^{-2}.

of sound. At the peak of the pulse the critical surface is about 90 μm away from the original target surface, thus the 1D approximation is no longer reliable.

It is also interesting to make a comparison with the results of Duston *et al.* [5] obtained at the same laser intensity and using a very detailed atomic model coupled with hydrodynamics, but again in the 1D approximation. In that work the profiles of T_e and n_e are similar to the ones given by our simulations. The He-δ/H-β ratio is about two times smaller than our experimental value, indicating higher electronic temperature. According to this comparison we conclude that the 1D approximation is a more restrictive condition for hydrodynamics simulation than the accuracy of the atomic model employed.

3·5. *Analysis of rear-face spectra.* – A typical rear-face X-ray spectrum from a 6μm Al foil is shown in fig. 5 (top). The ratio between rear-face and front-face line intensities is found to increase with wavelength. In contrast, in the case of a «cold» Al foil of the same thickness, not irradiated by laser light, the X-ray transmission would be greatly reduced on the long wavelength side of this spectral region due to the K photoabsorption edge at $\lambda = 7.96$ Å.

Hence we see that heating and ionization of the target material reduces its X-ray opacity allowing for a more efficient X-ray transmission through the foil. This reduction of opacity can be explained by taking into account the shift, towards higher energies, of the K-shell absorption edge with increasing ionization state; this causes the X-ray transmittivity to increase dramatically in the spectral region of interest.

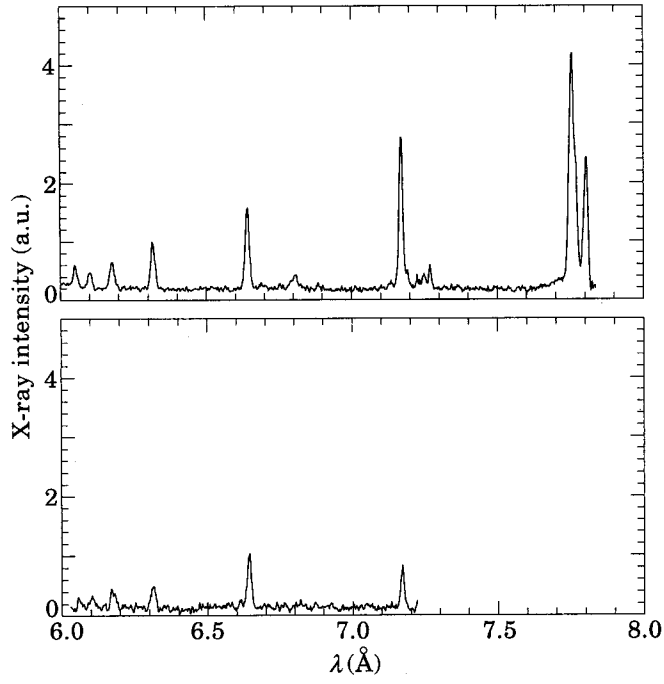

Fig. 5. – Rear-face X-ray spectra from a 6 μm Al foil (top) and from a 3 μm Al foil, filtered with a 3 μm Al filter (bottom).

The heating and ionization of the foil is determined by thermal and radiative energy transport beyond the critical surface, in the overdense plasma where the laser light cannot penetrate, and eventually in the cold target. As energy is transported through the foil, it heats up and gives rise to ionization, resulting in reduced inner-shell opacity at K-shell energies. This allows K-shell radiation from the frontside of the foil to penetrate deeper in the backside region.

The influence of energy transport on X-ray transmission was evidenced considering a rear-face spectrum from a 3 μm laser-irradiated foil, further filtered with a 3 μm foil placed between the first foil and the spectrometer. This last spectrum, also shown in fig. 5 (bottom), showed strongly reduced X-ray transmission, whose wavelength dependence was close to that expected for a «cold» 3 μm foil. This suggests that a significant fraction of the total target thickness is ablated during the X-ray emission process, confirming that energy transport involves a foil layer thicker than 3 μm. This conclusion is in agreement with accurate studies [5] which show that radiation is the most important energy transport mechanism in interaction conditions similar to ours. Thus it is the X-ray radiation itself that, heating the foil, drives its deeper penetration in the backside region.

4. – Conclusion.

We studied the X-ray spectrum of K-shell emission from both front and rear face of an Al foil irradiated by a Nd laser beam. Temperature and density of the X-ray emitting plasma were estimated by measurements of line intensity ratios. Comparison of the two spectra showed that the ratio between rear-face and front-face line intensities increases with wavelength in the 6–8 Å spectral region. This fact was explained observing that the X-ray transmittivity of the aluminium foil changes with the local temperature. The X-ray radiation emitted from the plasma produced at the surface irradiated by the laser beam, penetrates into the solid inner layers of the Al foil modifying its spectral transmittivity and making it more transparent to the primary X-ray radiation. This effect has to be further investigated for a deeper comprehension of radiation transport in dense plasmas. Moreover our observations suggest that rear-face X-ray emission from laser-irradiated metal foils can be used for applications at a rather high level of efficiency. This method will supply X-ray laser-plasma sources free from spurious laser radiation and ablation debris from the target.

* * *

We acknowledge the continuous and effective support of the IFAM technical staff.

REFERENCES

[1] KAUFFMANN R. L., in *Handbook of Plasma Physics 3*, edited by M. N. ROSENBLUTH and R. Z. SAGDEEV (North-Holland) 1992.
[2] SIGEL R., *Laser-induced radiation hydrodynamics*: X-*ray generation and application*, XLV SUSSP, St. Andrews (1994).
[3] ROSEN D., *Phys. Fluids*, 2 (1990) 1461.

[4] GIZZI L. A., GIULIETTI D., GIULIETTI A., AFSHAR-RAD T., BIANCALANA V., CHESSA P., DANSON C., SCHIFANO E., VIANA S. M. and WILLI O., *Phys. Rev. E*, **49** (1994) 5628.
[5] DUSTON D., CLARK R. W., DAVIS J. and APRUZESE J. P., *Phys. Rev. A*, **27** (1983) 1441.
[6] GIZZI L. A., BATANI D., BIANCALANA V., GIULIETTI A. and GIULIETTI D., *Laser Part. Beams*, **10** (1992) 65.
[7] ROCKETT P. D., BIRD C. R., HAILEY C. J., SULLIVAN D., BROWN D.B. and BURKHALTER P. G., *Appl. Opt.*, **24** (1985) 2536.
[8] HENKE B. L., LEE P., TANAKA T. J., SHIMABUKURO R. L. and FUJIKAWA B. K., *At. Data Nucl. Data Tables*, **27** (1982) 1.
[9] KELLY R. L., *J. Phys. Chem. Ref. Data*, **16**, Suppl. 1 (1987) 1372.
[10] HAUER A. A., DELAMATER N. D. and KOENIG Z. M., *Laser Part. Beams*, **9** (1991) 3.
[11] LEE R. W., WHITTEN L. and STOUT R. E., *J. Quant. Spectrosc. Radiat. Transfer*, **32** (1984) 91.
[12] DUSTON D. and DAVIS J., *Phys. Rev. A*, **21** (1980) 1664.
[13] BASTIANI S., GIULIETTI D., GIULIETTI A., GIZZI L.A., CECCOTTI T. and MACCHI A., *Proc. XXIII ECLIM, Oxford* (1994).
[14] CHRISTIANSEN J. P., ASHBY D. E. and ROBERTS K. V., *Comput. Phys. Commun.*, **7** (1974) 271; RODGERS P. A., ROGOYSKI A. M. and ROSE S. J., RAL report No.RAL-89-127 (1989).